Structure and elasticity of phlogopite under compression: Geophysical implications

Tanvi D. Chheda[1], Mainak Mookherjee[1], David Mainprice[2], Antonio M. dos Santos[3], Jamie J. Molaison[3], Julien Chantel[456], Geeth Manthilake[456], William A. Bassett[1]

[1] Earth and Atmospheric Sciences, Cornell University, Ithaca, NY 14853, United States

[2] Geosciences Montpellier UMR CNRS 5243, Universite Montpellier 2, 34095 Montpellier Cedex 05, France

[3] Neutron Sciences Directorate, Oak Ridge National Laboratory, Oak Ridge, TN 37831, United States

[4] Clermont Université, Université Blaise Pascal, Laboratoire Magmas et Volcans, BP 10448, F-63000 Clermont-Ferrand, France

[5] CNRS, UMR 6524, LMV, F-63038 Clermont-Ferrand, France

[6] IRD, R 163, LMV, F-63038 Clermont-Ferrand, France

Abstract

We investigated the response of the crystal structure, lattice parameters, and unit-cell volume of hydrous layered silicate phlogopite at conditions relevant to subduction zone settings. We have used first principles simulation based on density functional theory to calculate the equation of state and full elastic constant tensor. Based on the generalized gradient approximation, the full single crystal elastic constant tensor with monoclinic symmetry shows significant anisotropy with the compressional elastic constants: $c_{11} = 181$ GPa, $c_{22} = 185$ GPa, $c_{33} = 62$ GPa, the shear elastic constants $c_{44} = 14$ GPa, $c_{55} = 20$ GPa, $c_{66} = 68$ Ga, and $c_{46} = -6$ GPa; the off diagonal elastic constants $c_{12} = 48$ GPa, $c_{13} = 12$ GPa, $c_{23} = 12$ GPa, $c_{15} = -16$ GPa, $c_{25} = -5$ GPa and $c_{35} = -1$ GPa at zero pressure. The elastic anisotropy of phlogopite is lar- ger than most of the layered hydrous phases relevant in the subduction zone conditions. The shear anisotropy, AVS for phlogopite is ~77% at zero pressure condition and although it decreases upon com- pression it remains relatively high compared to other hydrous phases relevant in the subduction zone settings. We also note that the shear elastic constants for phlogopite are relatively low. Phlogopite also has a high isotropic bulk V_P/V_S ratio ~2.0. However, the V_P/V_S ratio also exhibits significant anisotropy with values as low as 1.49. Thus, phlogopite bearing metasomatized mantle could readily explain unusual V_P/V_S ratio as observed from seismological

studies from the mantle wedge regions of the subduction zone.

1. Introduction

Phlogopite is a potassium bearing mica that is stable in hydrous ultrapotassic rocks. In particular, phlogopite occurs in hydrother- mally altered oceanic crust and mantle. Phase stability studies show that phlogopite could be stable up to pressures of 9 GPa (Yoder and Eugster, 1954; Yoder and Kushiro, 1969; Kushiro et al., 1967; TrØnnes, 2002) and has been thought to play an important role in generation of arc magmas (Sudo and Tatsumi, 1990). However, more recent studies have shown that, during the breakdown of phlogopite much of the water is partitioned into potassium amphibole, richterite, owing to the similar K/OH ratio (Konzett and Ulmer, 1999). Only a small amount of aqueous fluid is released and this cannot account for the formation of the arc magmas (Konzett and Ulmer, 1999). The mantle wedge overlying subducting slabs is further hydrated by the release of such aqueous fluids. And at least a part of the incompatible elements such as potassium, partition into the released fluids that migrate upward and lead to widespread mantle metasomatism (Bailey, 1982). This stabilizes potassium bearing hydrated assemblages such as phlogopite bearing altered peridotite in the mantle wedge (Sekine and Wyllie, 1982; Wyllie and Sekine, 1982) overlying the subducted slabs. Also, sub-cratonic lithosphere might be enriched in large ion lithophile elements (such as potassium) through metasomatism by hydrous silicate melts (Thompson, 1992). The bulk chemical compositions of altered rocks such as mica-amphibole-rutile-ilmenite-diopside (MARID) is very similar to the chemistry of phlogopite in a $(Mg,Fe)_2SiO_4$ (olivine)–SiO_2 (quartz)–$K_2O + Na_2O$ (alkali) ternary (Sweeney et al., 1993). Hence, understanding the physical properties of phlogopite is likely to enhance our understanding of the thermodynamic stability of the altered rock assemblages. In addition, it is also important to con- strain the elasticity of phlogopite and evaluate its role in explain- ing geophysical observations in the subduction zone settings. Most of the studies conducted so far have focused on the phase relations (e.g., Konzett and Ulmer, 1999; Sato et al., 1996,1997; Fumagalli et al., 2009), crystal structure, and equation of state of phlogopite (Rayner, 1974; Hazen and Finger, 1978; Pavese et al., 2003; Comodi et al., 2004; Gatta et al., 2011). However, the full monoclinic elastic constant tensor of phlogopite has never been measured and till now, only the 5 independent constants of pseudo-hexagonal symmetry have been reported in the literature (Alexandrov and Ryzhova, 1961; Aleksandrov et al., 1974). In this study, we explore the crystal structure, equation of state, and full monoclinic elastic constant tensor of phlogopite at high-pressures using first principles simulation.

2. Method

2.1. First principle simulations

We performed first principles quantum mechanical simulation based on density functional theory (DFT) (Hohenberg and Kohn, 1964; Kohn and Sham, 1965). Density functional theory has been widely used to study the structure, energetics, and elasticity of mineral phases relevant to Earth and Planetary sciences (e.g., Oganov et al., 2002). The DFT solution for the energies in the system considered is exact in principle, but the nature of the elec- tronic many-body interaction is mapped onto a potential for exchange and correlation that needs to be approximated. We investigate phlogopite [K(Mg)3(Si3Al)O10(OH)2] with two widely used approximations to the exchange–correlation functional: the generalized gradient approximation (GGA) (Perdew and Wang, 1986; Perdew et al., 1991) and local density approximation (LDA) (Ceperley and Adler, 1980). We have used widely accepted and highly accurate projector augmented wave method (PAW) (Kresse and Joubert, 1999) as implemented in the Vienna ab initio

simulation package (VASP) (Kresse and Hafner, 1993; Kresse and Furthmuller, 1996a,b; Kresse and Joubert, 1999). We determined the energy–volume relationship of the phlogopite phase using GGA and LDA with PAW methods. Phlogopite has a monoclinic, C2/m space group symmetry (Redhammer and Roth, 2002). The aluminum and silicon atoms are ordered in the TO4 tetrahedral sites. Although our calculations are static, we have ordered the alu- minum and silicon atoms into the tetrahedral sites in distinct lay- ers and to retain the monoclinic symmetry we doubled the c-axis. All computations were performed in the primitive unit-cell with a space group P21/c with 88 atoms and Z = 4 (Fig. 1). We used an energy cut-off Ecut = 500 eV and a Monkhorst–Pack (Monkhorst and Pack, 1976) 2 2 2 k-point mesh, yielding 2 k points in the irreducible wedge of the Brillouin zone. A series of convergence tests demonstrated that these computational parameters yield total energies that converge within 5 meV/atom. Previous studies have shown that density functional theory captures the relevant physics of hydrous minerals (Mookherjee and Stixrude, 2006; Mainprice et al., 2008; Tsuchiya and Tsuchiya, 2009; Ortega-Castro et al., 2010; Chantel et al., 2012) with varying bond strengths from strong hydroxyls to the weak interlayer forces (Stackhouse et al., 2004; Fumagalli and Stixrude, 2007; Mookherjee and Stixrude, 2009; Mookherjee and Capitani, 2011; Militzer et al., 2011; Mookherjee and Bezacier, 2012; Hernandez- Haro et al., 2013). Based on previous computational studies GGA

often leads to more accurate predictions for the hydrogen bearing mineral systems (Tsuchiya et al., 2005, 2008; Mookherjee and Stixrude, 2006). In addition to hydrogen bearing minerals, compu- tational studies on molecular water (H2O) and ice (Hamann, 1997) show that the GGA method (Perdew et al., 1996) provided excel- lent predictions for energetics and elasticity of hydrogen bearing systems. However, LDA method has been successful in describing the equation of state of layered hydrous phases such as talc (Stixrude, 2002; Stixrude and Peacor, 2002). Hence, we calculated the full elastic constant tensor of phlogopite using both the GGA and LDA method. To calculate the elasticity, we strained the lattice and allowed the internal degrees of freedom of the crystal structure to relax consistent with the symmetry: elastic constants were obtained through the changes in stress tensor (r) with respect to applied strain (e). For a specific volume, we applied positive and negative strains of magnitude 0.5%, 1%, and 2% and accurately determined the stresses. The elastic constants were then determined by the linear relation between the stress and strain in the appropriate limit of zero strain (Fig. S1). We noted that 1% strain approximates   the limit of zero strain as previously reported for most of the geologically relevant mineral phases (Karki et al., 2001). Hence to remain in the field of linear elastic behavior we employed strains up to 1% to determine the elastic constants. An orthogonal reference frame used for computing the tensor may be X = a⁄ Y = b/b⁄ Z = c. We calculated the elastic anisotropy of phlogopite using petrophysical software (Mainprice, 1990).
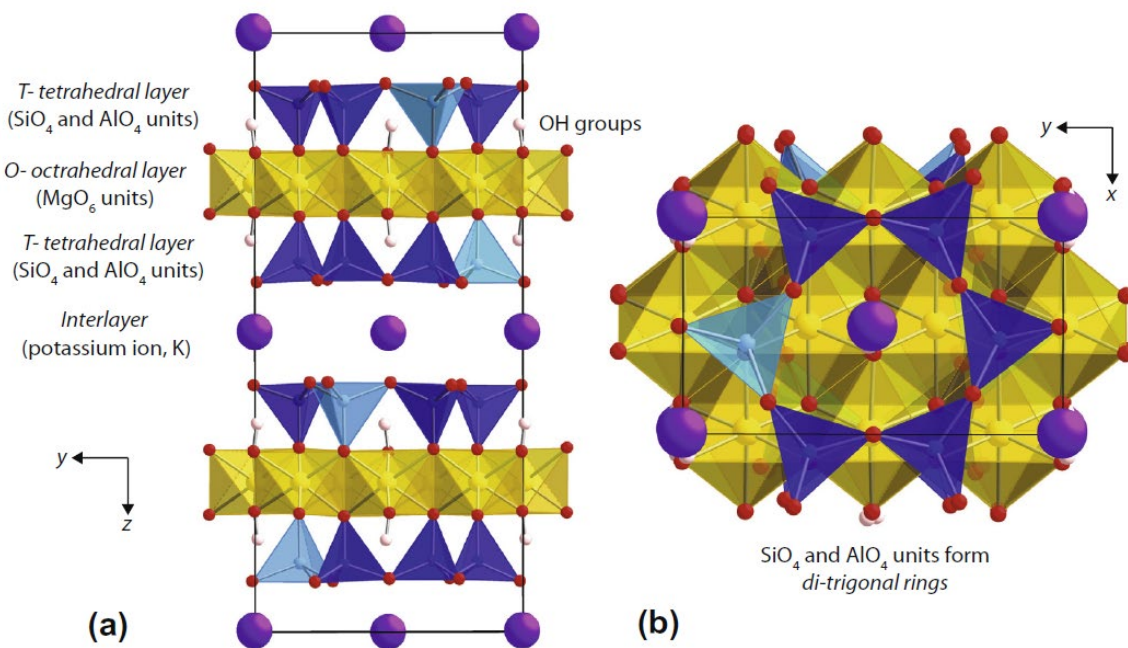

(a)   (b)

Fig. 1. Crystal structure of phlogopite with C2/m space group symmetry. TO4 tetrahedral units where T = Si, Al are arranged to form di-trigonal rings. Two such tetrahedral sheets with their tetrahedral apex pointing towards each other sandwich an octahedral layer. MO6 octahedral units are indicated by light yellow color where M = Mg. Interlayer region is occupied by potassium atoms. The silicon (Si) and aluminum (Al) atoms are shown as dark and light blue spheres respectively. The potassium (K) atoms are shown as purple large spheres. The hydrogen atoms are denoted as white spheres; the oxygen atoms are denoted as red spheres.

3. Result

3.1. Equation of state

The volume dependence of total energy obtained using DFT simulations with LDA and GGA approximations are adequately described by a third-order Birch–Murnaghan equation of state (Birch, 1978)

$$E = E_0 + \frac{9}{2}K_0 V_0 \left[(K_0' - 4)f_V^3 + f_V^2\right] \tag{1}$$

where, E0, K0, V0, and K'0 represents the ground state energy, bulk modulus at zero-pressure, unit-cell volume at zero-pressure, and pressure derivative of zero-pressure bulk modulus respectively. And, fv is the volume Eulerian finite strain, defined as,

$$f_V = \frac{1}{2}\left(\left(\frac{V_0}{V}\right)^{2/3} - 1\right) \tag{2}$$

Equation of state parameters for phlogopite.

E_0 [eV]	σ_{E0}	V_0 [Å³]	σ_{V0}	K_0 [GPa]	σ_{K0}	K'	$\sigma_{K'}$	Method
−652.44	0.05	473.03	1.06	60.8	4.3	8.1	1.7	LDA[a]
−595.30	0.04	518.72	1.08	41.6	2.5	10.1	1.3	GGA[a]
		488.64	0.20	49.7	0.5	8.6	0.2	SXRPD[b]
		497.10	0.10	54.0	2.0	7.0	1.0	SCXRD[c]
		487.70	0.20	58.5	2.0			SCXRD[d]

a this study; LDA: local density approximation, GGA: generalized gradient approximation.

b Pavese et al. (2003); SXRPD: synchroton X-ray powder diffraction.

c Comodi et al. (2004); SCXRD: single-crystal X-ray diffraction.

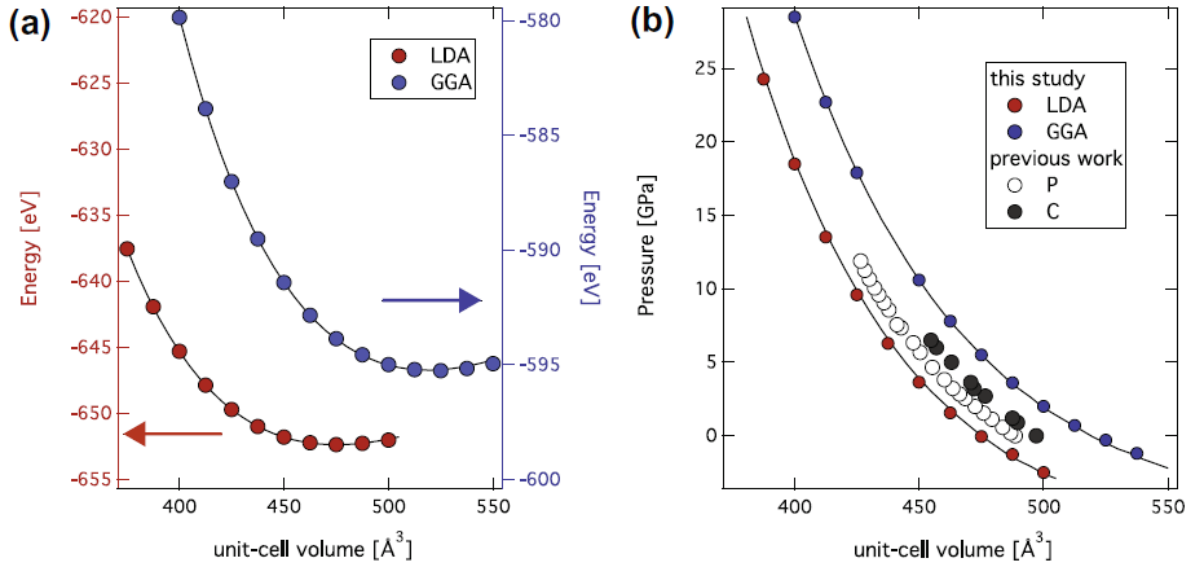d Hazen and Finger (1978); SCXRD: single-crystal X-ray diffraction.

Fig. 2. (a) Plot of energy with respect to unit-cell volume predicted by first principles. Legend: LDA- red symbols; GGA- blue symbols. (b) Plot of pressure vs. unit-cell volume. Experimental results- X-ray diffraction data are denoted by 'grey' (C- Comodi et al., 2004) and 'white' symbols (P- Pavese et al., 2003). First principles result from LDA (red symbols) and GGA (blue symbols) tend to bracket the experimental results. (For interpretation of the references to color in this figure legend, the reader is referred to the web version of this article.)
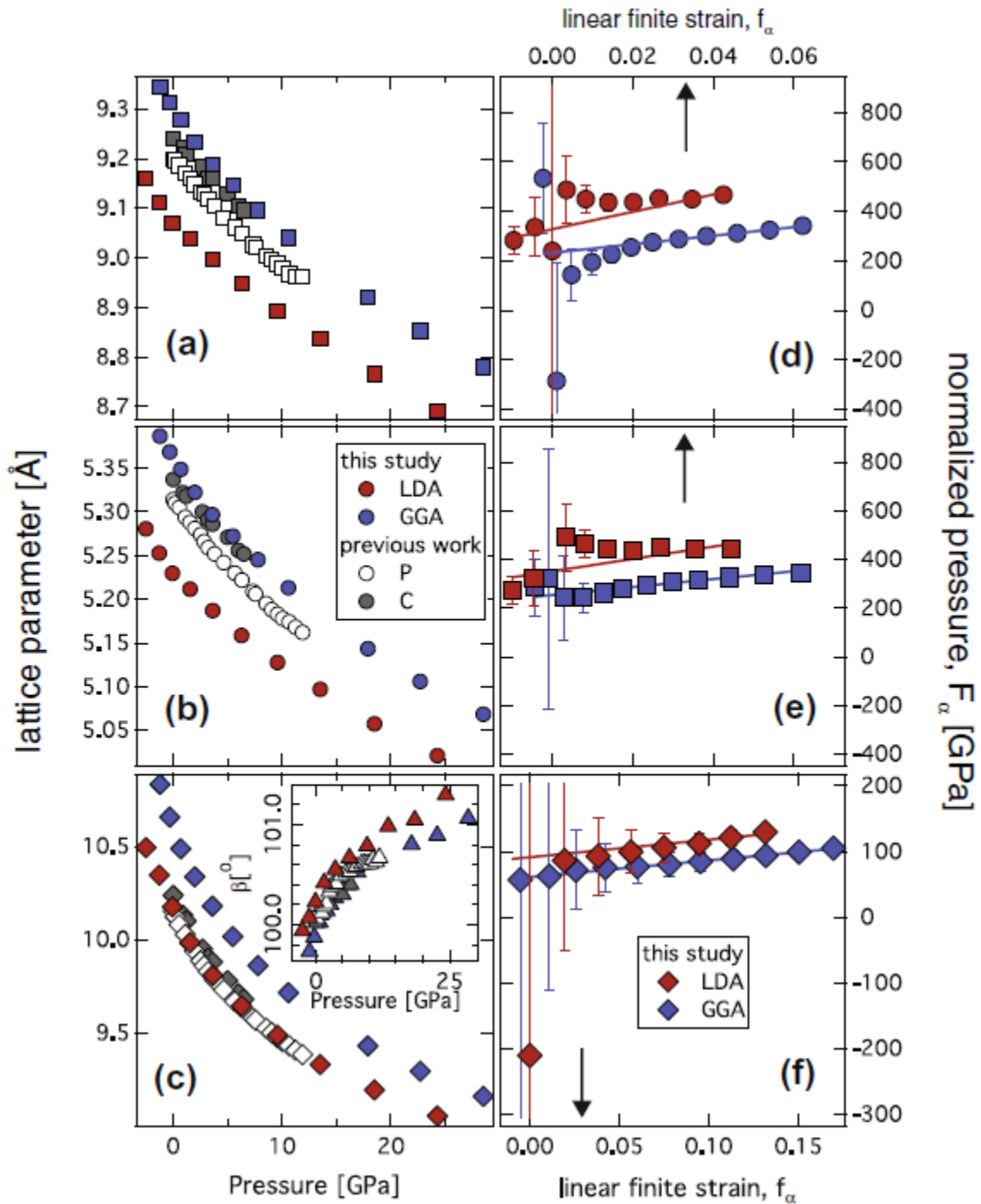
Fig. 3. Plot of the lattice parameters vs. pressure (a) a-axis, (b) b-axis, and (c) c-axis. Inset in the panel (c) also shows the plot of lattice parameter b vs. pressure. In panels (d– f), linear normalized pressure, Fl vs. the linear Eulerian finite strain, fl are plotted for a-axis, b-axis, and c⁄-axis. The intercept along the ordinate indicates the linear compressibility Ka, Kb and Kc. Data from previous X-ray diffraction studies are denoted by 'white' (C- Comodi et

al., 2004) and 'grey' (P-Pavese et al., 2003) symbols. The first principles simulation results from this study are denoted by 'red' (LDA) and 'blue' (GGA) symbols. (For interpretation of the references to color in this figure legend, the reader is referred to the web version of this article.)

3.2. Structure

Phlogopite is a layered hydrous silicate with tetrahedral units linked to form di-trigonal rings. An octahedral layer is sandwiched by two such tetrahedral sheets with the tetrahedral apex pointing heating, the interlayer region also undergoes significantly larger expansion compared to the other structural units (Mookherjee and Redfern, 2002). The main compression along the a–b plane is accommodated by in-plane rotation of tetrahedral units, character- ized by the angle, a. For a perfect hexagonal ring, a = 0°, as the hex- agonal ring deforms to di-trigonal ring where a > 0°. Upon compression, the degree di-trigonal distortion increases as shown by the increase of the angle as a function of pressure. Similar behaviour is also observed in previous single crystal X-ray diffraction study (Comodi et al., 2004) (Fig. 4). The behaviour of a upon com- pression is opposite when layered silicates expand on heating, i.e., a tends to decrease when a layered hydrous silicate undergo thermal expansion leading to decrease of the di-trigonal distortion (Mookherjee et al., 2001; Chon et al., 2006). Upon compression, the hydroxyl (OH) bond length (rOH) remains largely unchanged and the corresponding O—H and O—O distances, i.e., rO—H and rO—O decrease (Fig. 4). Within the pressure range of our study we do not find any evidence of hydrogen bonding since the OAH bond lengths do not increase upon compression, as documented in hydrogen-bonded systems.
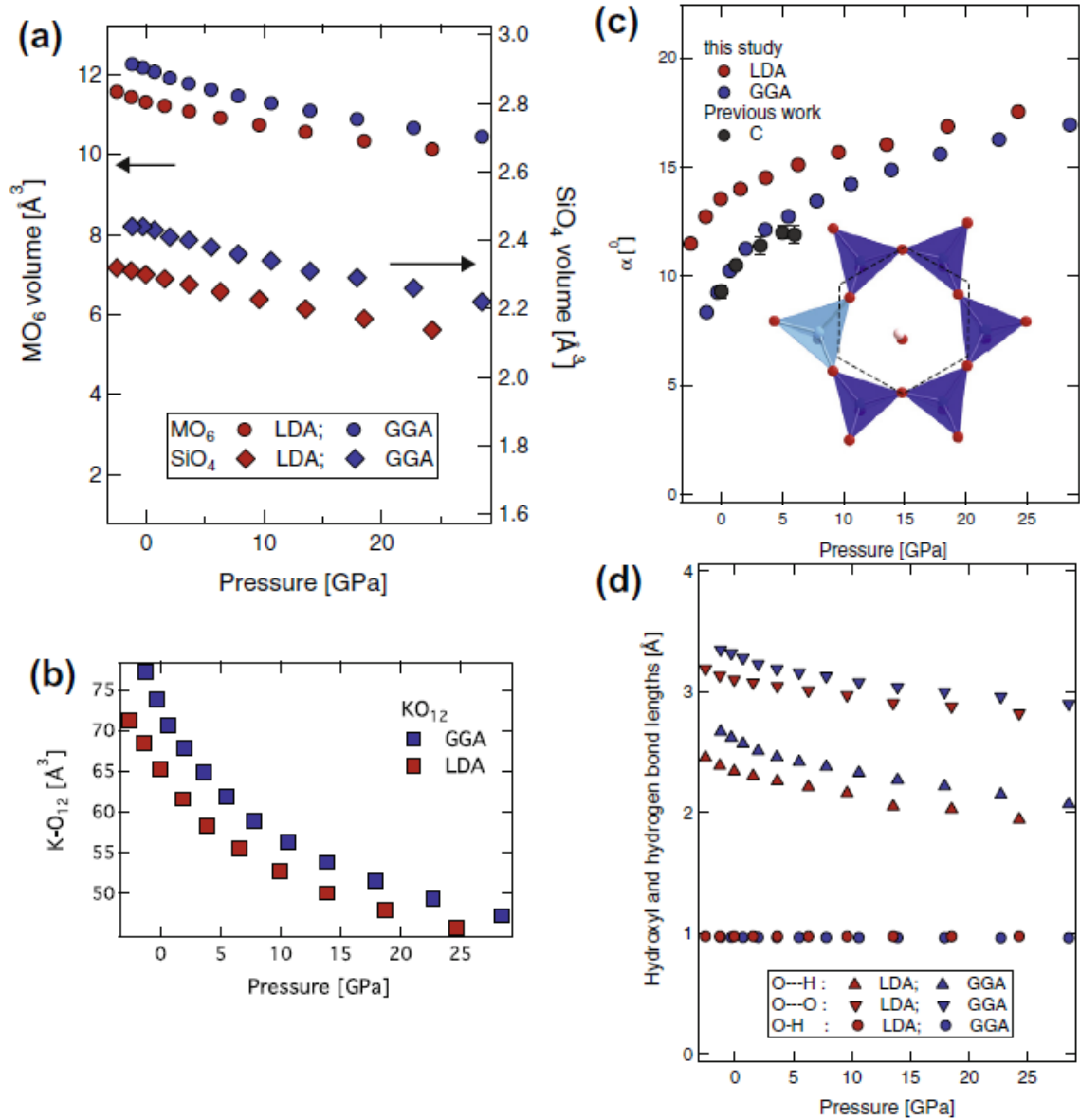
Fig. 4. Plot of volume of polyhedral units vs. pressures- (a) tetrahedral units- TO4 are represented in the right-ordinate axis; the octahedral units MO6 are represented in the left-ordinate axis; (b) the interlayer with 12-fold coordination (KO12) vs. pressure. The first principle simulations with LDA and GGA are shown in 'red' and 'blue' symbols respectively. (c) Plot of a vs. pressure. The a angle characterizes the in-plane rotation of tetrahedral units as shown in the inset- a perfect hexagon, shown in dashed line, the angle between consecutive oxygen atoms would be 120° and hence a = 0°. In contrast, for a di-trigonal ring of tetrahedral units, the angle between consecutive oxygen atoms is either greater than or less than 120° resulting in a > 0°. Under compression the di-trigonal distortion characterized by a, increases with pressure. The first principle simulations with LDA and GGA are shown in 'red' and 'blue' symbols respectively.

Data from previous X-ray diffraction studies are denoted by 'grey' (C- Comodi et al., 2004). (d) Plot of O–H, O—H and O—O distances with pressure. Within the compression range explored in this study there is no evidence for the formation of hydrogen bonds since O–H bond distances remain rather constant and do not increase in length, which is often diagnostic of hydrogen bonding. (For interpretation of the references to color in this figure legend, the reader is referred to the web version of this article.)

3.3. Elasticity

Phlogopite has monoclinic symmetry with 13 independent elas- tic constants, three compressional elastic constants- c11, c22, c33, three shear elastic constants- c44, c55, c66 and seven off diagonal elastic constants- c12, c13, c23, c15, c25, c35, and c46 (Nye, 1985). As a result of low symmetry and the rarity of obtaining gem quality single crystals, very few experimental data on the elasticity of phlogopite exist (Alexandrov and Ryzhova, 1961; Aleksandrov et al., 1974). The calculated elastic constants are in excellent agree- ment with the experimental data (Fig. 5). Among the principal elastic components- c11~c22 > c33, whereas the off-diagonal elastic constant show the relation- c12 > c13~c23 and c35 > c25 > c15. The shear elastic constants follow the relation- c66 > c55 > c44 > c46 (Fig. 5). The relationship holds for both LDA and GGA methods and all pressures.
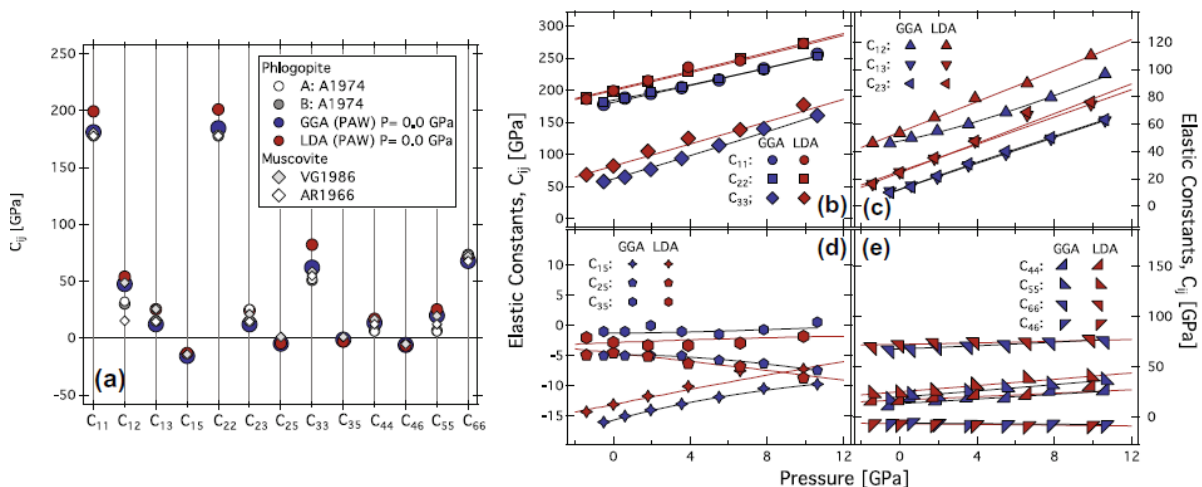

Fig. 5. (a) Comparison between experimental results and ab initio predicted elastic constants at room pressure. Experimental elastic tensor for two distinct phlogopite samples A and B

(A1974) (Aleksandrov et al., 1974) are compared with the results from this study. We also compare phlogopite single crystal elastic constants with muscovite. Muscovite single crystal elastic constant data are from VG1986 (Vaughan and Guggenheim, 1986); AR1961 (Alexandrov and Ryzhova, 1961). Elastic constants, c_{ij} as a function of pressure- (b) compressional components, c_{11}, c_{22} and c_{33}; (c) off-diagonal components, c_{12}, c_{13}, and c_{23}; (d) off-diagonal components, c_{15}, c_{25}, and c_{35}; (e) shear components, c_{44}, c_{55}, c_{46}, and c_{66}. The 'blue' and 'red' filled symbols from first principles simulation with GGA and LDA respectively. (For interpretation of the references to color in this figure legend, the reader is referred to the web version of this article.)

4. Discussion and conclusion

Until the first principles result presented here the only available set of elastic constants for phlogopite were those measured by Alexandrov and Ryzhova (1961) using ultrasonics at room pressure and later refined by Aleksandrov et al. (1974)). Two crystals were measured one from the Slyudyanka and other from Aldan region, near Lake Baikal, Russia. The experimental measurements were used to constrain the 5 independent elastic moduli with hexagonal symmetry rather than full 13 independent elastic moduli required for monoclinic symmetry of phlogopite. The refined experimental two crystals of Aleksandrov et al. (1974) are labeled, the values of the elastic constants of these two crystals agree very closely within 10 GPa despite the fact they come from regions that are separated by over 1000 km. The elastic constants from this study based on DFT agree with experimental values very closely within 15 GPa for c11, c22, c13, c23, c44, c55, and c66 for GGA. The predicted elastic constants for phlogopite using GGA are also similar to the elastic constants for muscovite determined using Brillouin scattering (Vaughan and Guggenheim, 1986) and ultrasonic method (Alexandrov and Ryzhova, 1961). Phlogopite is a tri-octahedral mica, i.e., all the three octahedral sites are occupied typically by a divalent cation (such as Mg^{2+}), whereas muscovite is a di-octahedral mica, where two of the three octahedral sites are occupied, typically by a trivalent cation (such as Al^{3+}). However, the remark- able similarity of the full elastic constant tensor between phlogopite and muscovite indicate that the elasticity is relatively insensitive of the exact chemistry of the octahedral sites.

Fig. 5b–e shows the evolution of the elastic constants with pressure, the compressional elastic constants c11~c22 > c33 increase with pressure. The softer c33 indicates the high compressibility normal to the basal plane. The shear moduli with the relation c44~c55 < c66 do not increase significantly with pressure. The nearly equal compressional components c11~c22 and shear

11

components c44 c55, are indications that the symmetry is close to hexagonal or transverse isotropic symmetry with quasi-isotropic behavior in the basal plane. The pressure dependence of the off-diagonal elastic constants is more complex as they have compressional and shear contributions. Phlogopite has extremely anisotropic elastic properties, as shown by the ab initio monoclinic elastic constant tenors. The c-axis is significantly more compressible than the a– b plane as expected for a layer silicate.
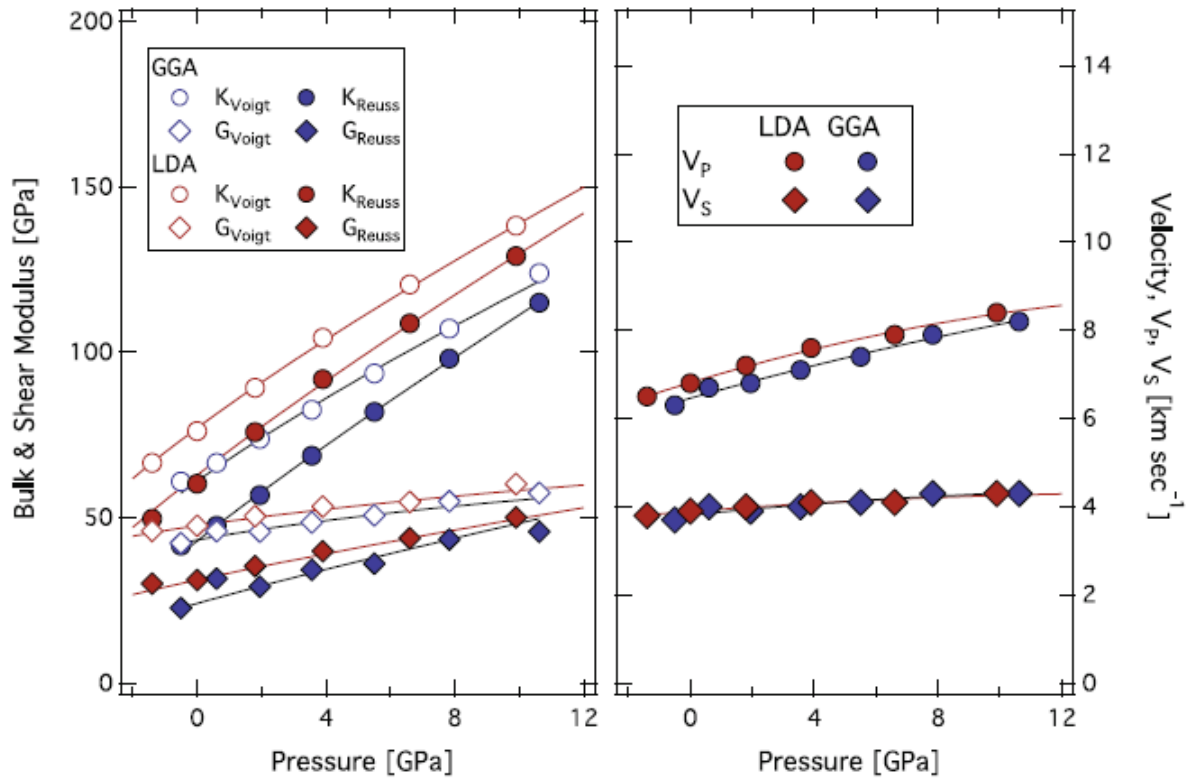

Fig. 6. (a) Plot of bulk and shear modulus vs. pressure. Both Voigt and Ruess bounds are shown. (b) Plot of compressional (V P), shear (VS) sound velocity vs. pressure. The 'blue' and 'red' filled symbols from first principles simulation with GGA and LDA respectively. (For interpretation of the references to color in this figure legend, the reader is referred to the web version of this article.)

The isotropic bulk and shear modulus stiffen for both GGA and LDA results based on first principles method (Fig. 6). As a result, the VP and VS also increases as a function of pressure. However, the pressure derivative for the shear modulus is lower than for the bulk modulus.

The seismic properties calculated using both the previous experimental and DFT based elastic constants illustrates the simi- larity in the results using the monoclinic and pseudo-hexagonal symmetry tensors (Fig. 7), with high VP and shear wave anisotropy in the basal plane. The monoclinic nature of phlogopite is reflected in the mirror symmetry plane (north–south direction in the stereo- plot, Fig. 7) normal to the b-axis, which is most clearly seen on the S-wave anisotropy (AVS) and VS1 polarization plots. Compared to the experimental elastic constants with pseudo-hexagonal symmetry, the anisotropy is lower by ~10% for VP and ~20% for VS for the DFT based elastic constants with monoclinic symmetry. This reflects the simplification of the velocity distribution introduced by the pseudo-hexagonal symmetry.
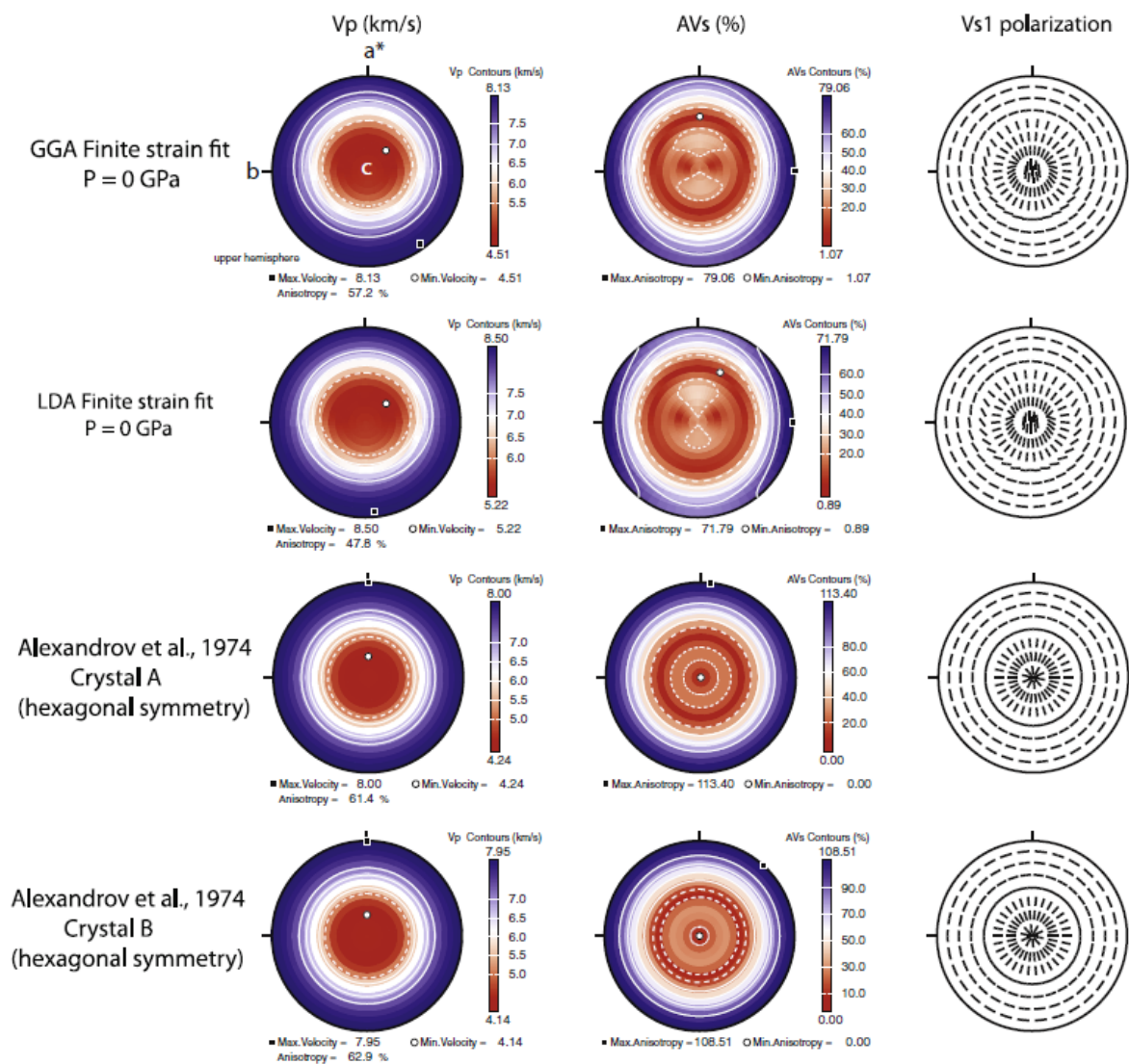

Fig. 7. Stereo plot of ab initio predicted seismic anisotropy at 0 GPa: AV P, AV S% and VS1 polarization for GGA, LDA methods (this study), also shown are plots from the elastic constants

13

from previous experiments (Aleksandrov et al., 1974).

At zero-pressure conditions, the talc has a maximum AVP of 80% and that of chlorite has a minimum AVP of 30%. At these conditions, the P-wave anisotropy, AVP of antigor- ite, brucite, and phlogopite are quite similar. Upon compression beyond 5–6 GPa, i.e., beyond the high-pressure stability of chlorite, talc, and antigorite, AVP of phlogopite is maximum. At zero-pressure conditions, talc and phlogopite have the largest S-wave anisotropy with AVS between 80–85%. Upon compression, the AVS of both talc and phlogopite reduces. However, the rate of reduction of talc is significantly greater than that of phlogopite. In contrast, the AVS of both chlorite and antigorite tends to increase upon com- pression. However, within the pressure stability region of chlorite and antigorite (i.e., below 5 GPa), phlogopite has greater AVS. Beyond the high-pressure stability region of chlorite and antigorite (P > 6 GPa), AVS of chlorite and antigorite are greater than that of phlogopite, however these phases are unlikely to be stable. Hence, AVS of phlogopite is likely to play a dominant role.

Owing to the wide range of pressure–temperature stability, i.e., pressures up to 9 GPa and temperatures up to 1400 °C (TrØnnes, 2002), Phlogopite micas could occur at wide variety of settings such as in upper mantle with normal mantle geotherm and sub- duction zone settings. Phlogopite rich bearing ultrapotassic MARID type of rocks (up to 90% phlogopite) have been reported as nodules in kimberlites from continental cratons (Waters, 1987). These phlogopite bearing MARID rocks may occur at the lithosphere asthenosphere boundary (LAB), which is characterized by intense metasomatism (O'Reilly and Griffin, 2010). If the mantle flow beneath the LAB is essentially horizontal, i.e., parallel to the LAB then the MARID rocks with large modal fractions of phlogopite is likely to orient its (001) horizontal layers parallel to the LAB. The resulting vertical VP is likely to be slow and the S-wave anisotropy
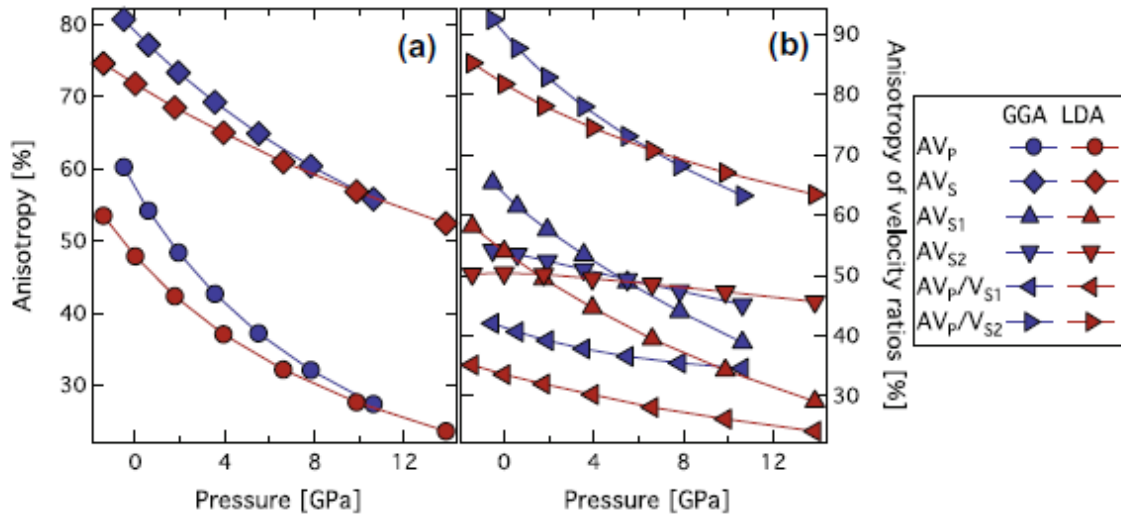
Fig. 8. Plot of seismic anisotropy for phlogopite, (a) AVP and AVS% (b) AVS1 , AVS2 , AVP =VS1 , and AVP =VS2 as a function of pressure.
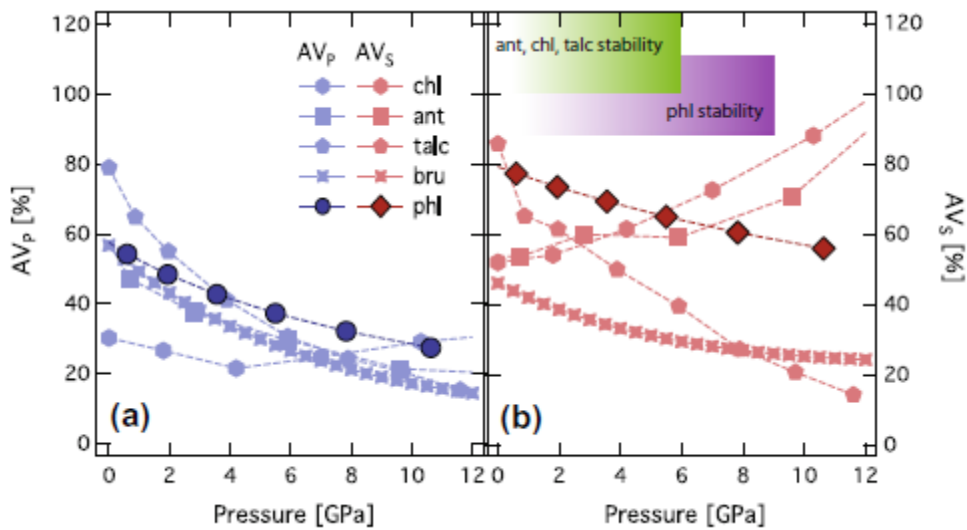

Fig. 9. Plot of (a) P-wave anisotropy, AV P and (b) S-wave anisotropy, AV S for various hydrous phases relevant for the subduction zone settings, as a function of pressure. Mineral abbreviations: chl- chlorite (Mookherjee and Mainprice, 2014), ant- antigorite- serpentine polymorph (Mookherjee and Capitani, 2011), tlc- talc (Mainprice et al., 2008), bru- brucite (Jiang et al., 2006). The light green shaded area represents the high-pressure stability field of antigorite,

chlorite, and talc (Mainprice and Ildefonse, 2009 and references therein), the light purple shaded area represents the high-pressure stability field for phlogopite (TrØnnes, 2002) (For interpretation of the references to color in this figure legend, the reader is referred to the web version of this article.).

The subduction zone settings are likely to be characterized by significant hydration and thus stabilizing variety of hydrous phases including phlogopite. The anisotropy of the layered hydrous sili- cates such as talc (Stixrude, 2002; Mainprice et al., 2008) and antigorite (Bezacier et al., 2010; Mookherjee and Capitani, 2011) are significantly larger than the major mantle phases such as oliv- ine. In certain subduction zones such as Ryukyu, in addition to the trench parallel shear wave polarization anisotropy, a large delay time has been observed (Long and Silver, 2008). To explain such a large delay time of around 1–2 s with a peridotitic rock domi- nated by olivine, one would require a significant thickness of around 100–150 km. Owing to the large anisotropy layered silicates are plausible candidates (Katayama et al., 2009; Bezacier et al., 2010; Mookherjee and Capitani, 2011). Although layered hydrous silicate minerals tend to have similar crystal preferred ori- entations due to the very strong control of their layered structure. Typical CPO pattern is a strong alignment of the basal plane with foliation plane of the rock and the weak alignment of a- or b- direc- tions may also occur in the foliation plane. This has been observed in series of earlier studies (Katayama et al., 2009; Lloyd et al., 2009; Jung, 2011; Padron-Navarta et al., 2012). To our knowledge, at present, experimental study of slip systems of phlogopite is lack- ing. The elastic anisotropy is also dominated by very strong control of the layered structure as illustrated by the similarity between muscovite and phlogopite. Based on these arguments on the deformation fabric, together with the seismic-anisotropy, a modest 10–15 km thick layer could explain both the trench parallel shear wave polarization anisotropy and a large delay time. The mantle wedge in the subduction zone settings are charac- terized by a V_P/V_S ratio ranging between 1.76 and 1.82 (Zhang et al., 2004; Syracuse et al., 2008; Tsuji et al., 2008). Recent high- resolution measurement of seismic velocities in subduction zone settings have revealed unusually low V_P/V_S ratios ranging from 1.65 to 1.72 (Wagner et al., 2005, 2006, 2008; Rossi et al., 2006; Eberhart-Phillips et al., 2006). A unique combination of ray path and anisotropy is required to explain such unusual V_P/V_S ratios. It is known that the mantle wedge is severely altered owing to release of fluids from dehydrating minerals in the subducting slabs. Although, fluids tend to stabilize layered hydrous silicate phases such as antigorite, chlorite, and phlogopite, these layered minerals typically have an isotropic $V_P=V_S \sim 2:0$. Olivine, the dominant mantle mineral may explain such an unusual V_P/V_S 1.65–1.72 when [100] axis of olivine is oriented

perpendicular to rather than seismic ray at higher angles w.r.t. (001) planes seismic ray (teleseismic) near parallel to planes parallel to the ray path (Hacker and Abers, 2012). We find that the anisotropy of the phlogopite at a density of ~2.79 gm/cm3 is such that the VP/VS1 ratios are as low as 1.5 (Fig. 10) and hence these hydrous phases such as phlogopite could also explain the unusual VP/VS ratios, in addition to the dominant peridotitic rocks.
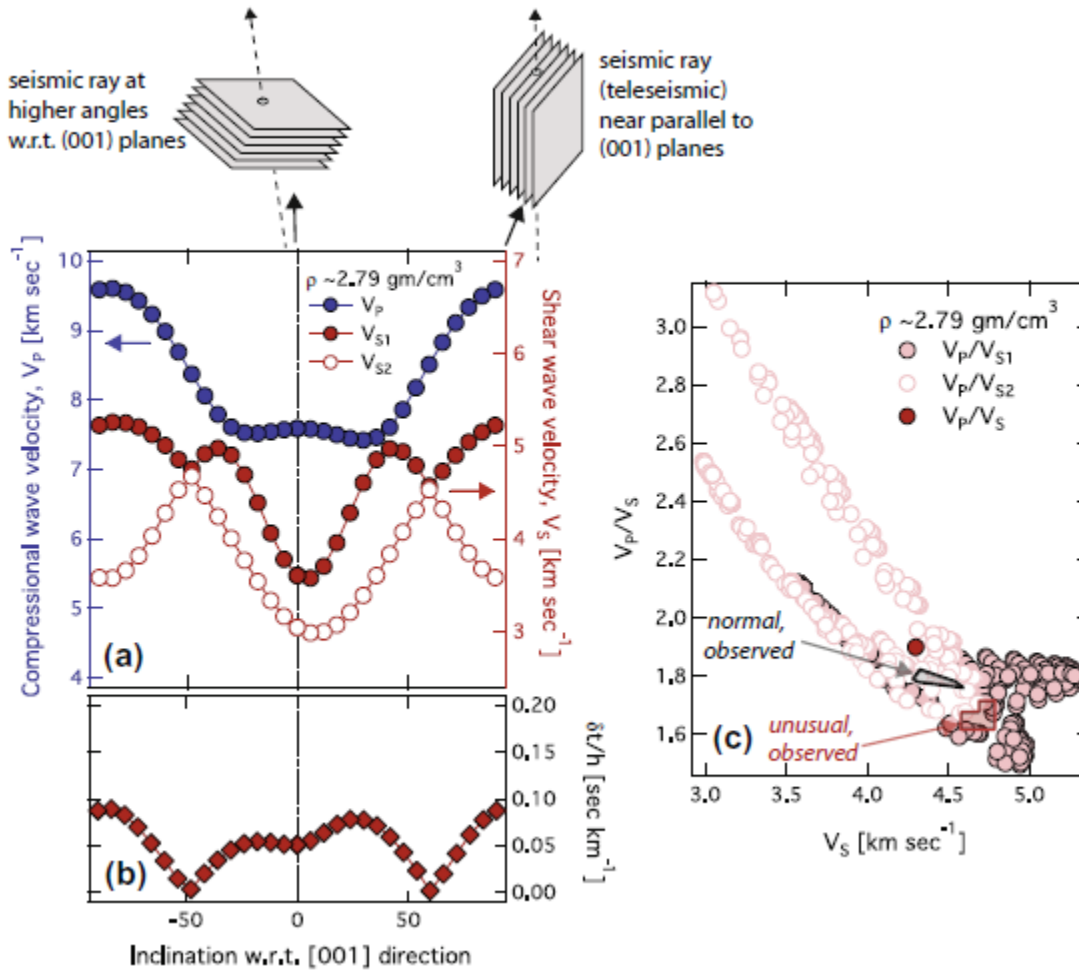

Fig. 10. (a) Variation of compressional (VP), shear (VS) sound velocity as a function of orientation with respect to the [001] direction. (b) Plot of delay time/layer thickness [dVS/(VS1 x VS2)] as a function of as a function of the angle of incidence between the seismic ray path and (001) plane of phlogopite. In the top, the layered hydrous silicates with the stacking of (001) planes are shown with the seismic rays oriented nearly perpendicular, i.e., seismic rays are almost aligned with the [001] direction. Also shown are the stacking of (001) planes and seismic rays are almost aligned with plane i.e., nearly perpendicular to the [001] direction. (c) Plot of

17

VP/VS ratio as a function of VS for phlogopite at a density of 2.79 gm/cm3. Since there is significant anisotropy the P-wave and S-wave (VS1; VS2) for all propagation directions are plotted, the spread in the VP/ VS1 and VP/VS2 results from the large anisotropy. Also shown is the isotropic VP/VS (filled red symbol). Two regions marked as 'usual, observed' (grey) and 'unusual, observed' (red) represents the seismological observations in mantle wedges (modified from Hacker and Abers, 2012). Once the anisotropy of hydrous phases are taken into account, the hydrous phases such as phlogopite could readily explain the unusual observations of VP/VS in subduction zones.

Acknowledgements

Appendix A. Supplementary data

Supplementary data associated with this article can be found, in the online version, at http://dx.doi.org/10.1016/j.pepi.2014.05.004.

References

Aleksandrov, K.S., Alchikov, U.V., Belikov, B.P., Zaslavskii, B.I., Krupnyi, A.I., 1974. Velocities of elastic waves in minerals at atmospheric pressure and increasing precision of elastic constants by means of EVM (in Russian). Izv. Acad. Sci. U.S.S.R. Geol. Ser. 10, 15–24.

Alexandrov, K.S., Ryzhova, T.V., 1961. Elastic properties of rock-forming minerals II. Layered Silicates. Bull. Acad. Sci. U.S.S.R. Geophys. Ser. 9, 1165–1168.

Bailey, D.K., 1982. Mantle metasomatism – continuing chemical change within the earth. Nature 296, 525–550.

Bezacier, L., Reynard, B., Bass, J.D., Sanchez-Valle, C., Van de Moortele, B., 2010. Elasticity of antigorite, seismic detection of serpentinites, and anisotropy in subduction zones. Earth

Planet. Sci. Lett. 289, 198–208.

Birch, F., 1978. Finite strain isotherm and velocities for single-crystal and polycrystalline NaCl at high pressures and 300 K. J. Geophys. Res. 83, 1257– 1268.

Ceperley, D.M., Adler, B.J., 1980. Ground state of the electron gas by a stochastic method. Phys. Rev. Lett. 45, 566–569.

Chantel, J., Mookherjee, M., Frost, D.J., 2012. The elasticity of lawsonite at high pressure and the origin of the low velocity layers in subduction zones. Earth Planet. Sci. Lett. 349–350, 116–125.

Chon, C.M., Lee, C.K., Song, Y., Kim, S.A., 2006. Structural changes and oxidation of ferroan phlogopite with increasing temperature: in situ neutron powder diffraction and Fourier transform infrared spectroscopy. Phys. Chem. Miner. 33, 289–299.

Comodi, P., Fumagalli, P., Montagnoli, M., Zanazzi, P.F., 2004. A single-crystal study on the pressure behavior of phlogopite and petrological implications. Am. Mineral. 89, 647–653.

Davies, G.F., 1974. Effective elastic-moduli under hydrostatic stress. 1. Quasi- harmonic theory. J. Phys. Chem. Solids 35, 1513–1520.

Eaton, D.W., Darbyshire, F., Evans, R.L., Grütter, H., Jones, A.G., Yuan, X., 2009. The elusive lithosphere-asthenosphere boundary (LAB) beneath cratons. Lithos 109, 1–22.

Eberhart-Phillips, D., Christensen, D.H., Brocher, T.M., Hansen, R., Rupert, N.A., Haeussler, P.J., Abers, G.A., 2006. Imaging the transition from Aleutian subduction to Yakutat collision in central Alaska, with local earthquakes and active source data. J. Geophys. Res. 111, B11303.

Fumagalli, P., Stixrude, L., 2007. The 10-angstrom phase at high pressure by first principles calculations and implications for the petrology of subduction zones. Earth Planet. Sci. Lett. 260, 212–226.

Fumagalli, P., Zanchetta, S., Poli, S., 2009. Alkali in phlogopite and amphibole and their effects on phase relations in metasomatized peridotites: a high-pressure study. Contrib. Mineral. Petrol. 158, 723–737.

Gatta, G.D., Merlini, M., Rotiroti, N., Curetti, N., Pavese, A., 2011. On the crystal chemistry and elastic behavior of a phlogopite 3T. Phys. Chem. Miner. 38, 655– 664.

Hacker, B.R., Abers, G.A., 2012. Subduction factory 5: unusually low Poisson's ratios in subduction zones from elastic anisotropy of peridotite. J. Geophys. Res. 117, B06308.

Hamann, D.R., 1997. H2O hydrogen bonding in density functional theory. Phys. Rev. B 55, R10157–R10160.

Hazen, R.M., Finger, L.W., 1978. The crystal structures and compressibilities of layer minerals

at high pressure II. Phlogopite and chlorite. Am. Mineral. 63, 293–296. Hernandez-Haro, N., Ortega-Castro, J., Del Valle, C.P., Munoz-Santiburico, D., Sainz-

Diaz, C.I., Hernandez-Laguna, A., 2013. Computational study of the elastic behavior of the 2M1 muscovite-paragonite series. Am. Miner. 98, 651–664.

Hohenberg, P., Kohn, W., 1964. Inhomogenous electron gas. Phys. Rev. B 136, B864– 871.

Jiang, F., Speziale, S., Duffy, T.S., 2006. Single-crystal elasticity of brucite, Mg(OH)2, to 15 GPa by Brillouin scattering. Am. Mineral. 91, 1893–1900.

Jung, H., 2011. Seismic anisotropy produced by serpentine in mantle wedge. Earth Planet. Sci. Lett. 307, 535–543.

Karki, B.B., Stixrude, L., Wentzcovitch, R.M., 2001. Elastic properties of major mantle materials of earth's mantle from first principles. Rev. Geophys. 39, 507–534.

Katayama, I., Hirauchi, K.-I., Michibayashi, K., Ando, J.-I., 2009. Trench-parallel anisotropy produced by serpentine deformation in hydrated mantle wedge. Nature 461, 1114–1117.

Kohn, W., Sham, L.J., 1965. Self-consistent equations including exchange and correlation effects. Phys. Rev. 140, 1133–1138.

Konzett, J., Ulmer, P., 1999. The stability of hydrous potassic phases in lherzolitic mantle- an experimental study to 9.5 GPa in simplified and natural bulk compositions. J. Petrol. 40, 629–652.

Kresse, G., Furthmuller, J., 1996a. Efficiency of ab-initio total energy calculations for metals and semiconductors using a plane-wave basis set. Comput. Mater. Sci. 6, 15–50.

Kresse, G., Furthmuller, J., 1996b. Efficient iterative schemes for ab initio total- energy calculations using a plane-wave basis set. Phys. Rev. B 54, 11169–11186. Kresse, G., Hafner, J., 1993. Ab initio molecular-dynamics for liquid-metals. Phys.

Rev. B 47, 558–561.

Kresse, G., Joubert, D., 1999. From ultrasoft pseudopotentials to the projector augmented-wave method. Phys. Rev. B 59, 1758–1775.

Kushiro, I., Akimoto, S., Syono, Y., 1967. Stability of phlogopite at high pressures and possible presence of phlogopite in the earth's upper mantle. Earth Planet. Sci. Lett. 3, 197–203.

Lloyd, G.E., Butler, R.W.H., Casey, M., Mainprice, D., 2009. Mica, deformation fabrics and the seismic properties of the continental crust. Earth Planet. Sci. Lett. 288, 320–328.

Long, M.D., Silver, P.G., 2008. The subduction zone flow field from seismic anisotropy. Science 319, 315–318.

Mainprice, D., 1990. A fortran program to calculate seismic anisotropy from the lattice preferred orientation of minerals. Comput. Geosci. 16, 385–393.

Mainprice, D., Ildefonse, B., 2009. Seismic anisotropy of subduction zone minerals – contribution of hydrous phases. In: Lallemand, Serge, Funiciello, Francesca (Eds.), Frontiers in Earth Sciences' Subduction Zone Dynamics. Springer, doi 10.1007/978-3-540-87974-9.

Mainprice, D., Le Page, Y., Rodgers, J., Jouanna, P., 2008. Ab inito elastic properties of talc from 0 to 12 GPa: interpretation of seismic velocities at mantle pressures and prediction of auxetic behavior at low pressure. Earth Planet. Sci. Lett. 274, 327–338.

Meade, C., Jeanloz, R., 1990. Static compression of $Ca(OH)_2$ at room temperature: observations of amorphization and equation of state measurements to

10.7 GPa. Geophys. Res. Lett. 17, 1157–1160.

Militzer, B., Wenk, H.-R., Stackhouse, S., Stixrude, L., 2011. First-principles calculation of the elastic moduli of sheet silicates and their application to shale anisotropy. Am. Mineral. 96, 125–137.

Monkhorst, H.J., Pack, J.D., 1976. Special points for Brillouin-zone integrations. Phys. Rev. B13, 5188–5192.

Mookherjee, M., Bezacier, L., 2012. The low-velocity layer in subduction zone: structure and elasticity of glaucophane at high pressures. Phys. Earth Planet. Inter. 208–209, 50–58.

Mookherjee, M., Capitani, G.C., 2011. Trench parallel anisotropy and large delay times: elasticity and anisotropy of antigorite at high pressures. Geophys. Res. Lett. 38, L09315. http://dx.doi.org/10.1029/2011GL047160.

Mookherjee, M., Mainprice, D., 2014. Unusually large shear wave anisotropy for chlorite in subduction zone settings. Geophys. Res. Lett. 41. http://dx.doi.org/10.1002/2014GL059334.

Mookherjee, M., Redfern, S.A.T., 2002. A high-temperature Fourier transform infrared study of the interlayer and Si-O stretching region in phengite 2M1. Clay Miner. 37, 323–336.

Mookherjee, M., Stixrude, L., 2006. High-pressure proton disorder in brucite. Am. Mineral. 91, 127–134.

Mookherjee, M., Stixrude, L., 2009. Structure and elasticity of serpentine at high- pressure. Earth Planet. Sci. Lett. 279, 11–19.

Mookherjee, M., Redfern, S.A.T., Zhang, M., 2001. Thermal response of structure and hydroxyl ion of phengite- 2M1: an in situ neutron diffraction and FTIR study. Eur. J. Mineral. 13, 545–555.

Nye, J.F., 1985. Physical Properties of Crystals. Oxford University Press, Clarendon. Oganov, A. R., Brodholt, J. P., Price, G. D., 2002. Ab initio theory of thermo-elasticity and phase

transitions in minerals. In: Gramaccioli, C.M. (Ed.), Energy Modelling in Minerals, European Mineralogical Union Notes in Mineralogy, vol. 4. pp. 83– 170.

O'Reilly, S.Y., Griffin, W.L., 2010. The continental lithosphere-asthenosphere boundary: Can we sample it? Lithos 120, 1–13.

Ortega-Castro, J., Hernandez-Haro, N., Timon, V., Sainz-Diaz, C.I., Hernandez- Laguna, A., 2010. High-pressure behavior of 2M1 muscovite. Am. Mineral. 95, 249–259.

Padron-Navarta, J.A., Tommasi, A., Garrido, C.J., Sanchez-Vizcaino, V.L., 2012. Plastic deformation and development of antigorite crystal preferred orientation in high-pressure serpentinites. Earth Planet. Sci. Lett. 349–350, 75–86.

Pavese, A., Levy, D., Curetti, N., Diella, V., Fumagalli, P., Sani, A., 2003. Equation of state and compressibility of phlogopite by in-situ high-pressure X-ray powder diffraction. Eur. J. Mineral. 15, 455–463.

Perdew, J.P., Wang, Y., 1986. Accurate and simple density functional for the electronic exchange energy: generalized gradient approximation. Phys. Rev. B 33, 8800–8802.

Perdew, J.P., Chevary, J.A., Vosko, S.H., Jackson, K.A., Pederson, M.R., Singh, D.J., Fiolhais, C., 1991. Atoms, molecules, solids, and surfaces: applications of the generalized gradient approximation for exchange and correlation. Phys. Rev. B 46, 6671–6687.

Perdew, J.P., Burke, K., Erzerhof, M., 1996. Generalized gradient approximation made simple. Phys. Rev. Lett. 77, 3865–3868.

Rayner, J.H., 1974. The crystal structure of phlogopite by neutron diffraction. Mineral. mag. 39, 850–856.

Redhammer, G.J., Roth, G., 2002. Single-crystal refinements and crystal chemistry of synthetic trioctahedral micas KM3(Al3+, Si4+)4O10(OH)2, where M = Ni2+, Co2+, Fe2+, or Al3+. Am. Mineral. 87, 1464–1476.

Rossi, G., Abers, G., Rondenay, S., Chiristensen, D.H., 2006. Unusual mantle Poission's ratio, subduction, and crustal structure in central Alaska. J. Geophys. Res. 111, B09311.

Sato, K., Katsura, T., Ito, E., 1996. Phase relations of phlogopite with and without enstatite up to 8 GPa: implication to potassic magmatism and mantle metasomatism. Tech. Rep. ISEI Ser. A 65.

Sato, K., Katsura, T., Ito, E., 1997. Phase relations of natural phlogopite with and without enstatite up to 8 GPa: implication for mantle metasomatism. Earth Planet. Sci. Lett. 146, 511–526.

Sekine, T., Wyllie, P.J., 1982. Phase relationships in the system KAISiO4-Mg2SiO4- SiO2-H2O as a model or hybridization between hydrous siliceous melts and Peridotite. Contrib.

Mineral. Petrol. 79, 368–374.

Smyth, J.R., Jacobsen, S.D., Swope, R.J., Angel, R.J., Arlt, T., Domanik, K., Holloway, J.R., 2000. Crystal structures and compressibilities of synthetic 2M1 and 3T phengite micas. Eur. J. Mineral. 12, 955–963.

Stackhouse, S., Coveney, P.V., Benoit, D.M., 2004. Density functional theory based study of the dehydroxylation behavior of aluminous dioctahedral 2:1 layer type clay minerals. J. Phys. Chem. B108, 9685–9694.

Stixrude, L., 2002. Talc under tension and compression: spinodal instability and structure at high pressure. J. Geophys. Res. 107, B 001684.

Stixrude, L., Peacor, D.R., 2002. First principles study of illite-smectite and implications for clay mineral systems. Nature 420, 165–168.

Sudo, A., Tatsumi, Y., 1990. Phlogopite and K-amphibole in the upper mantle: implication for magma genesis in subduction zones. Geophys. Res. Lett. 17, 29– 32.

Sweeney, R.J., Thompson, A.B., Ulmer, P., 1993. Phase relations of a natural MARID composition and implications for MARID genesis, lithospheric melting and mantle metasomatism. Contrib. Mineral. Petrol. 115, 225–241.

Syracuse, E.M., Abers, G.A., Fischer, K., MacKenzie, L., Rychert, C., Protti, M., Gonzalez, V., Strauch, W., 2008. Seismic tomography and earthquake locations in the Nicaraguan and Costa Rican upper mantle. Geochem. Geophys. Geosys. 9, Q07S08.

Thompson, A.B., 1992. Water in the Earth's upper mantle. Nature 358, 295–302.

TrØnnes, R.G., 2002. Stability range and decomposition of potassic richterite and phlogopite end members at 5–15 GPa. Mineral. Petrol. 74, 129–148.

Tsuchiya, J., Tsuchiya, T., 2009. Elastic properties of d -AlOOH under pressure-first principle investigation. Phys. Earth Planet. Inter. 174, 122–127.

Tsuchiya, J., Tsuchiya, T., Tsuneyuki, S., 2005. First-principles study of hydrogen bond symmetrization of phase D under high pressure. Am. Mineral. 90, 44– 49.

Tsuchiya, J., Tsuchiya, T., Wentzcovitch, R.M., 2008. Vibrational properties of d- AlOOH under pressure. Am. Mineral. 93, 477–482.

Tsuji, Y., Nakajima, J., Hasegawa, A., 2008. Tomographic evidence for hydrated oceanic crust of the Pacific slab beneath northeastern Japan: implication for water transportation in subduction zones. Geophys. Res. Lett. 35, L14308.

Vaughan, M.T., Guggenheim, S., 1986. Elasticity of muscovite and its relationship to crystal structure. J. Geophys. Res. 91, 4657–4664.

Wagner, L.S., Beck, S.L., Zandt, G., 2005. Upper mantle structure in the South-Central Chilean

subduction zone (30 to 36S). J. Geophys. Res. 110, B01308.

Wagner, L.S., Beck, S.L., Zandt, G., Ducea, M., 2006. Depleted lithosphere, cold, trapped asthenosphere, and frozen melt puddles above the flat slab in Central Chile and Argentina. Earth Planet. Sci. Lett. 245, 289–301.

Wagner, L.S., Anderson, M.L., Jackson, J., Beck, S.L., Zandt, G., 2008. Seismic evidence for orthopyroxene enrichment in the continental lithosphere. Geology 36, 935– 938.

Waters, F.G., 1987. A suggested origin of MARID xenoliths in kimberlites by high- pressure crystallization of an ultrapotassic rock such as lamproite. Contrib. Mineral. Petrol. 95, 523–533.

Weaver, J.S., 1976. Application of finite strain theory to non-cubic crystals. J. Phys.

Chem. Solids 37, 711–718.

Wyllie, P.J., Sekine, T., 1982. The formation of mantle phlogopite in subduction zone hybridization. Contrib. Mineral. Petrol. 79, 375–380.

Yoder, H.S., Eugster, H.P., 1954. Phlogopite synthesis and stability range. Geochim.

Cosmochim. Acta 6, 167–185.

Yoder, H.S., Kushiro, I., 1969. Melting of a hydrous phase: phlogopite. Am. J. Sci. 267- A, 558– 583.

Zhang, H., Thurber, C.H., Shelly, D., Ide, S., Beroza, G.C., Hasegawa, A., 2004. High-resolution subducting slab structure beneath Northern Honshu, Japan, revealed by double-difference tomography. Geology 32, 361–364.